8

Theoretical studies of $Cu_2ZnGe(S/Se)_4$ absorbers using density functional theory

8.1 Introduction

Copper based quaternary chalcogenides CZTS/Se are attractive compound semiconductors with potential for optical devices mainly as absorbers in solar cell. However, the maximum efficiency reported for CZTS,Se solar cell is not improving beyond 12.7%. The researchers are coming with several different approaches to overcome the challenges/issues associated with CZTS/Se such as high voltage deficit, high interfacial and bulk recombination, inferior back contact etc [G. K. Gupta et al., 2018]. Thus, there is a need to look out for other prominent absorbers with desirable electronic and optical properties, suitable for high performance solar devices. Ge based quaternary chalcogenides recently attracted attention because of their similar structural properties like CZTS/Se. Incorporating Ge in place of Sn proportionally increases the band gap of absorber and with complete Sn replacement i.e. Cu_2ZnGeS_4 (CZGS) and $Cu_2ZnGeSe_4$ (CZGSe) materials show bandgap of (1.9 - 2.2 eV) and (1.29 - 1.63 eV), respectively [Caballero et al., 2014][Ã, Ochiai, & Katsui, 2005][Schleich & Wold, 1977][Matsushita, Maeda, Katsui, & Takizawa, 2000][Levcenko et al., 2015]. Thus, favorable optical properties and bandgap tunability make CZGS/Se a potential candidate for single junction and also tandem cell geometries. The partial substitution of Sn with Ge in CZTS/Se improves the device open circuit voltage, which is the bottleneck for kesterite devices [Bag, Gunawan, Gokmen, Zhu, & Mitzi, 2012][Hages et al., 2013][Collord & Hillhouse, 2016]. Already, an efficiency up to 10.1% has been reached with Ge alloyed CZTS absorber layers [Giraldo et al., 2015]. A monolithic tandem cell, using kesterite (CZTS,Se) bottom cell and perovskite ($CH_3NH_3PbI_3$) top cell. is fabricated with about 1.35 V open circuit voltage and 4.6% efficiency with projected maximum efficiency above 16% [T. Todorov, Gershon, Gunawan, Sturdevant, & Guha, 2014]. Ge based high bandgap kesterite (CZGS) can be a potential choice as top cell absorber to realize efficient kesterite tandem cells. Further, improvement in the device performance has been reported by using a graded bandgap structure from 4.8% for pure CZTGS to 6.3% using graded bandgap CZTGS absorber [I. Kim et al., 2014]. These reports suggests a possible pathway for efficiency improvement by implying different composition ratio of cations (x) and anions (y) in $Cu_2ZnGe_{1-x}Sn_xS_{1-y}Se_y$ for absorbers in graded and tandem structure solar cells. Apart from the advantages of bandgap tunability, replacing Sn with Ge also is advantageous as Ge, is less likely to change its oxidation states as compared to the multivalent Sn in CZTS,Se lattice. This reduces the possibility of enhanced recombination centers and thus, may increase carrier carrier life time in CZGS,Se as compared to CZTS,Se system [Biswas et al., 2010][G. K. Gupta et al., 2018]. However, in spite of several possibilities for improvements towards future photovoltaics, not much attention has been given to CZGS/Se compound semiconductor discussing their detailed structural, optical and electronic properties, which are pivotal in understanding/explaining their photovoltaic response.

Present chapter discusses the electronic and optic properties of CZTS/Se quaternary compound semiconductor in its Kesterite (space group I-4) and Stannite (space group I-42m) crystallographic phases, calculated using density functional theory (DFT) approach. Electronic properties of these materials are investigated in terms of their electronic band structure and

density of states. The optical properties such as dielectric constant, refractive index, reflectivity and absorption coefficient are computed and discussed.

8.2 Computational details

We used the density functional theory based full potential linearized augmented plane wave (FP-LAPW) method as implemented in Wien2k [Blaha, Schwarz, & Madsen, 2001] to compute the structural, electronic and optical properties of CZGS and CZGSe quaternary compound semiconductor in their kesterite (I-4) and stannite (I-42m) phases. Strucutal optimization is done using the generalized gradient approximation (GGA) with Perdew, Burke, and Ernzerhof (PBE) type parameterization as exchange-correlation potentials. We have also used the modified Becke-Johnson (mBJ) exchange-correlation potential to mitigate the GGA deficiencies such as underestimation of bandgap. The muffin tin radii of atom are chosen sufficiently large to avoid any charge leakage from the atoms' core region. The value of product $R_{MT}*K_{max}= 7$ (R_{MT} is the smallest atomic radii and K_{max} is the largest K vector) and $G_{max}= 12$ are considered for structural optimization and 1000 K point are used for throughout the calculations. The convergence criteria for SCF calculation are 0.0001 Ry and 0.001e for energy and force, respectively.

8.3 Result and discussion

8.3.1 Structural properties

CZGS/Se materials have a tetragonal structure with kesterite (I-4) and stannite (I-4 2m) crystallographic phases. The lattice parameters of CZGS/Se systems in the kesterite and stannite phases are optimized by varying the volume of the unit cells with respect total energy. The computed total energy versus volume of cell for kesterite and stannite CZGS/Se phases are plotted in **Figure 8.2**. and optimized crystallographic structure are shown in **Figure 8.1**. The optimized structural parameters such as lattice constants, atomic positions and bond length are listed in **Table 8.1**. These results are in agreement with the reported computational and experimental (wherever available) results.

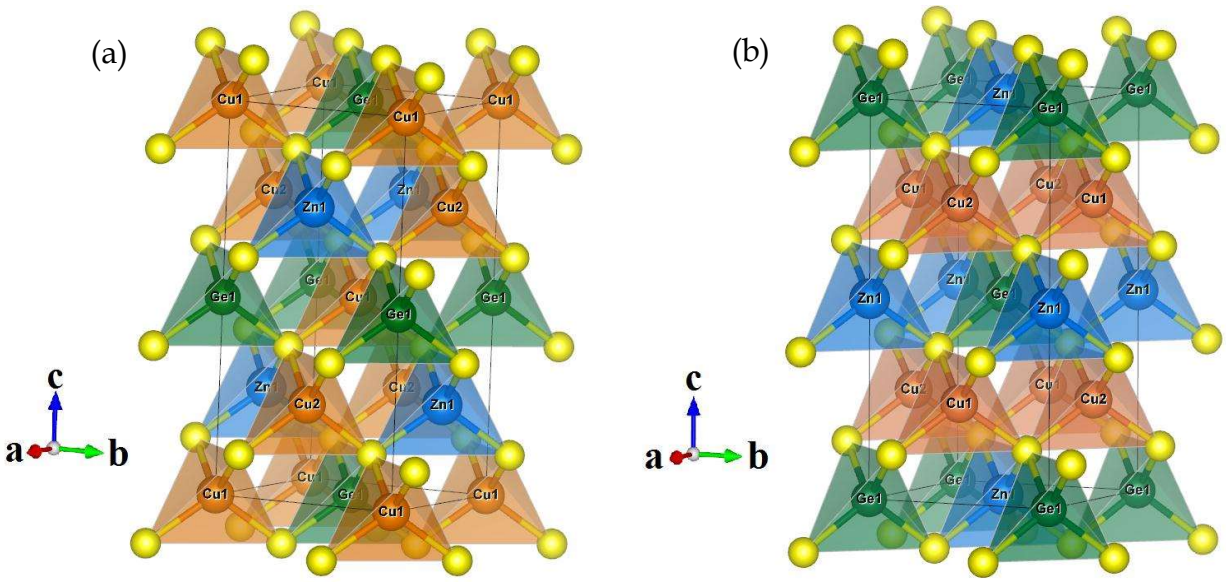

Figure 8.1 CZGS/Se crystal structure for (a) kesterite phase (Space group I-4) and (b) stannite phase (Space group I-4 2m) showing cations at the center of tetrahedron and chalcogens at the corner of tetrahedron

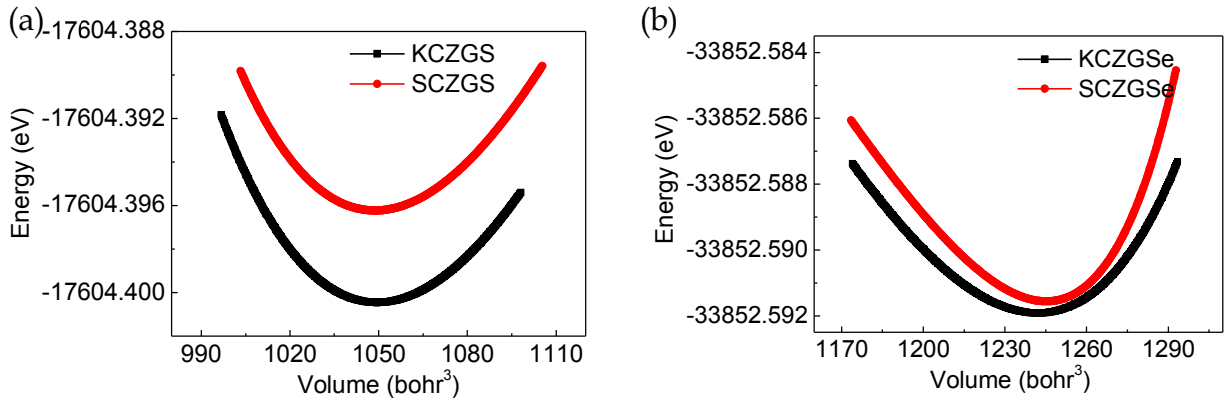

Figure 8.2 Volume optimization data, fitted with Murnaghan equation of state for (a) CZGS and (b) CZGSe in kesterite and stannite crystallographic phase

Cu-Ge and Cu-Zn cation layers lie one after the other in kesterite phase while Zn-Ge layer appears alternatively after the Cu-Cu layer in the stannite phase [Schorr, 2011]. The atoms are occupied in the respective Wyckoff positions as per their kesterite and stannite space group. The anion atoms S/Se form the tetrahedrons with cation atoms, as shown in **Figure 8.1**.

Table 8.1 Lattice parameter, bond length and anion S/Se atomic positions for CZGS/Se kesterite and stannite crystallographic phases

	KCZGS	SCZGS	KCZGSe	SCZGSe
a=b (Å)	5.38572, 5.358[c],5.334[i],5.3904[i]	5.37537,5.3[a],5.328[b],5.333[c],5.34[f]	5.713,5.672[c],5.5929[i]	5.68742, 5.6[a],5.583[b],5.652[c],5.606[d,g],5.622[e],5.592[h]
c/2a	0.97435,0.993[c],0.9863[i], 0.998[i]	1.0006,1.01[a],1.008[b],1.007[c],1.05[f]	0.98705,0.993[c],0.9863[i]	1.003, 1.014[b],1.005[a],1.003[c],0.9848[d,g],0.9836[e],0.9886[h]
x	0.24799	0.24383,0.2586[f]	0.24276	0.24612, 0.2557[g]
y	0.25684	x	0.25331	X
z	0.12328	0.12792,0.1230[f]	0.124945	0.13090,0.1237[g]
δCu1-S/Se	2.33159	2.31055,2.313[f]	2.45019,2.3976[j]	2.42705,2.425[g]
δCu2-S/Se	2.31008	2.31055,2.313[f]	2.4287,2.4276[j]	2.42705,2.425[g]
δZn-S/Se	2.365	2.3845,2.344[f]	2.49863,2.4742[j]	2.52988,2.445[g]
δGe-S/Se	2.3014	2.30852,2.234[f]	2.47621,2.3716[j]	2.47977,2.371[g]

[a]Reference[N. Sarmadian, Saniz, Partoens, & Lamoen, 2016], [b]Reference[D. Chen & Ravindra, 2013], [c]Reference[S. Chen, Gong, Walsh, & Wei, 2009], [d]Reference[Matsushita et al., 2000], [e]Reference[Schafer &

Nitsche, 1974], [f]Reference[Parasyuk et al., 2005] [g]Reference[Parasyuk, Gulay, Romanyuk, & Piskach, 2010], [h]Reference[Swapna Mary et al., 2016], [i]Reference[Khadka & Kim, 2013], [j]Reference[Litvinchuk, 2016]

We found that energy of kesterite crystallographic phase is lower energy than that of stannite phase CZGS/Se, thus, confirming that kesterite phases are more stable as compared to their stannite counterparts. This suggests that the formation of kesterite phases may be relatively easier under equilibrium growth condition. Similar result also have been reported for CZTS/Se material by [Persson, 2010][Ghosh, Thangavel, & Rajagopalan, 2013]. Lattice parameters ratio for is c/2a < 1 for kesterite phase and is >1 for stannite phase. This is similar to the CZTS/Se system. However, there are discrepancies with these observations, where some experimental studies reported that c/2a < 1 for stannite crystallographic phase [Schafer & Nitsche, 1974][Parasyuk et al., 2010][Swapna Mary et al., 2016]. The limited experimental studies are available for kesterite CZGS/Se phase and difficult to point out the exact relation between lattice parameters [Khadka & Kim, 2013]. The discrepancies in the c/2a ratio of kesterite and stannite phases are attributed due to approximately same atomic radii of Cu and Zn atoms. So it becomes difficult to differentiate between kesterite and stannite crystallographic phase. In addition, any observed experimental deviation from the theoretical c/2a ratio for stannite phase may be due to the co-existence of both kesterite and stannite phases. This is possible due to the very small energy difference between these two structures or due to the disordered Cu/Zn lattices in these structures.

8.3.2 Electronic properties

The electronic properties of kesterite and stannite CZGS/Se systems are discussed using their electronic band structure and density of states computed using the modified BJ exchange correlation potentials. Electronic band structures are plotted along the Γ→H→N→Γ symmetric points in irreducible Brillouin zone and Fermi energy is set at 0 eV and shown in **Figure 8.3**. Kesterite and stannite CZGS/Se systems are showing that conduction band minima (CBM) and valence band maxima (VBM) are located at Γ, confirming the direct bandgap semiconductor behavior. Kesterite phase based CZGS/Se system exhibit higher bandgap as compared to respective stannite phases. Similar results are also reported for kesterite and stannite CZTS/Se systems [Persson, 2010]. Se based kesterite and stannite phase materials exhibit higher band gap as compared to S based systems due to the fact that VBM of these structures are basically composed of hybridized Cu-3d and p states of the anion S or Se. Further, heavier atoms exhibit shallower atomic levels in the valence band maxima that's why a band reduction is noticed [D. Chen & Ravindra, 2013]. The computed electronic band structure and bandgap are also compared with other reported result, as listed in **Table 8.2**. The computed results are in in agreement with [S. Chen et al., 2009][Kodan, Auluck, & Mehta, 2016].

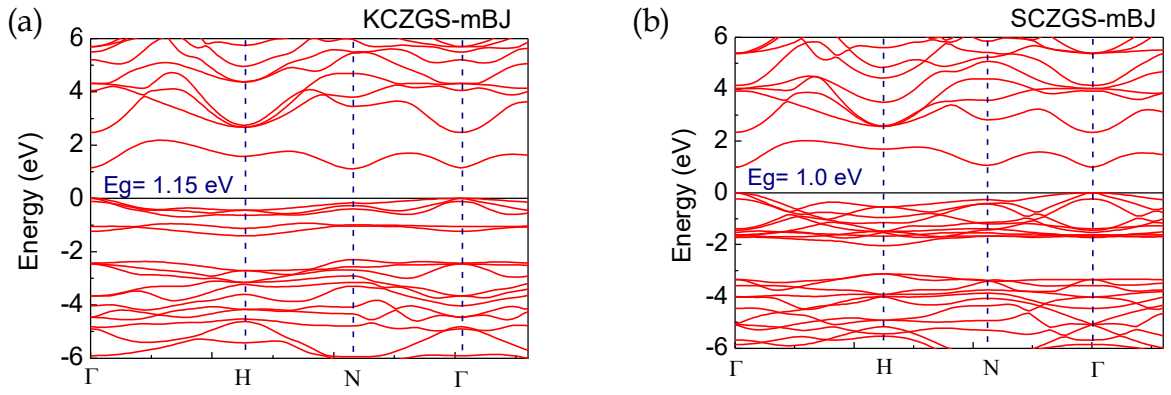

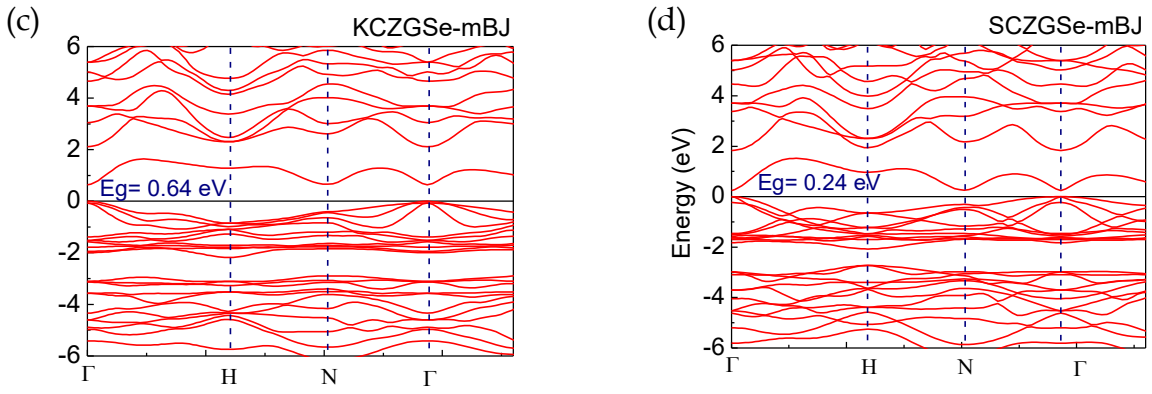

Figure 8.3 Band structure of CZGS/Se system for (a) kesterite CZGS, (b) stannite CZGS, (c) kesterite CZGSe and (d) stannite CZGSe

To understand in more detail about the electronic properties, we also computed the total and partial density of states in the range of -6 to 6 eV for kesterite and stannite CZGS/Se systems and shown in **Figure 8.4**. Bandgap observed by total density of states is similar to the bandgap values, observed by the electronic band structure. The contribution of different atomic orbitals in the valence and conduction bands are nearly same in the both kesterite and stannite phase of CZGS/Se system. Electronic states near the Fermi energy of valence band are mainly contributed by the Cu-d orbital and S/Se-p orbital for kesterite and stannite CZTS/Se systems. While electronic states in the conduction band near the Fermi energy are dominated by Ge-p and S/Se-p orbitals, showing strong coupling between them. The cations in kesterite and stannite phases form the tetragonal symmetry with S/Se anions that is substantiated by the observed strong hybridization of anion and cation atomic orbitals in the respective DOS spectra.

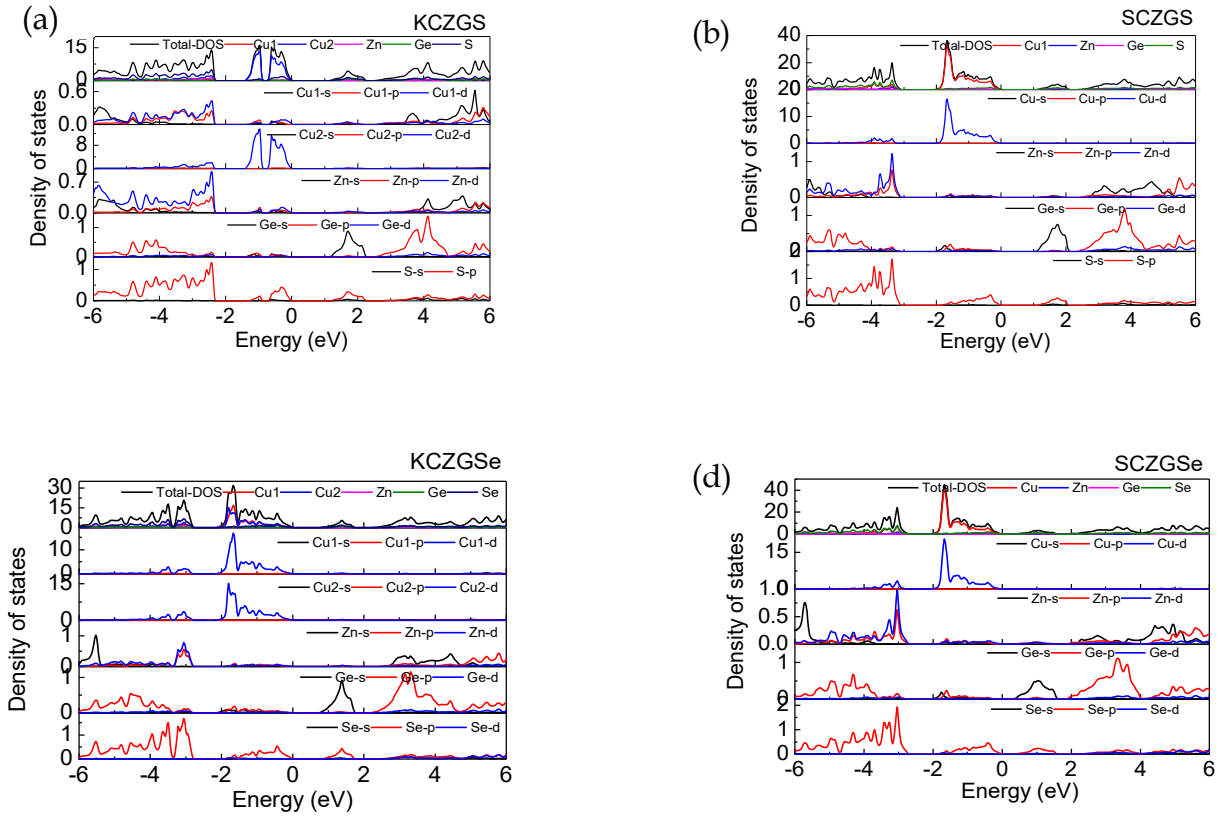

Figure 8.4 Total density of states and projected density of states for (a) kesterite CZGS (b) stannite CZGS (c) kesterite CZGSe (d) Stannite CZGSe

8.3.3 Optical properties

The kesterite and stannite CZGS/Se phases are showing tetragonal crystallographic structure, thus, leading to the anisotropic behavior along X and Z polarization direction. This is also evident from the computed optical properties. The real and imaginary parts of dielectric function are plotted along XX and ZZ directions for kesterite and stannite CZGS/Se systems.

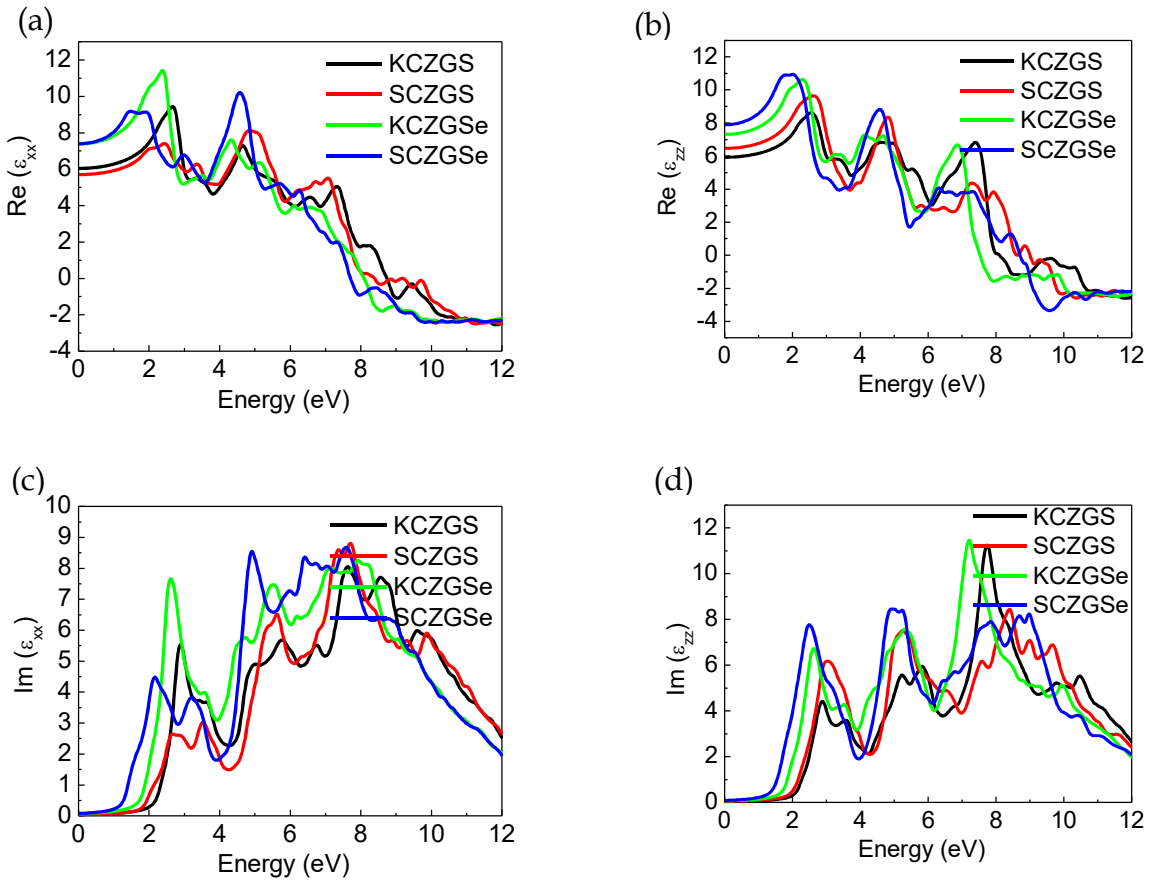

Figure 8.5 Dielectric constants as a function of energy for kesterite and stannite CZTS/Se phases: (a) real xx component; (b) real zz component; (c) imaginary xx component and (d) imaginary zz component

The imaginary component (Imε) of the dielectric function is calculated using the momentum matrix elements integrating over the Brillouin zone and further the real part of complex dielectric function are computed using the applying Kramers- Kronig transformation [Blaha et al., 2001]. Imaginary part of dielectric function is proportional to the absorption coefficient. The static dielectric constants are computed at zero energy along XX and ZZ direction. The static dielectric constant parallel to c-axis is higher than static dielectric constant in perpendicular direction for stannite and smaller for kesterite CZTS/Se phases. This is in agreement with previous reports [Nasrin Sarmadian, Saniz, Partoens, & Lamoen, 2016]. The values of static dielectric constant are computed by averaging in all the three crystallographic direction and listed in **Table 8.2**. Further, Imaginary part of dielectric function is showing similar dispersion behavior for kesterite and stannite CZGS/Se systems except the relative shift in the energy due to their different bandgap values, **Figure 8.5**. We further used 1 eV scissor correction for comparing the computed results with the experimental observations.

Table 8.2 Dielectric constants along c-axis $\varepsilon_{||}$ (ε_{zz}) and perpendicular to c-axis $\varepsilon_{\perp}$ (ε_{xx}), static dielectric constant ε_o, refractive index n, extinction coefficient, Δn, mBJ band gap values Eg_{mBJ}, band gap values after scissor corrections $Eg_{mBJ\_scissor}$ and experimental values $Eg_{Experimental}$ from literature for comparison.

Material	$\varepsilon^{\perp}$	$\varepsilon_{\parallel}$	ε_o	n	K	Δn	Eg_{mBJ} (eV)	$E_g$after scissor correction $Eg_{mBJ\ scissor}$ (eV)	Experimental band gap $Eg_{Experimental}$ (eV)
KCZGS	6.04016	5.92875	6.003	2.45	0.00963	-0.02277	1.15	2.1	1.88-2.23[g]
SCZGS	5.70463	6.46543	5.95823	2.44	0.00960	0.15429	1.0	2.02	2.16-2.24[j]
KCZGSe	7.38954	7.30861	7.36256	2.71	0.01308	-0.01492	0.64	1.77	1.17-1.52[d,g]
SCZGSe	7.39799	7.89264	7.56287	2.75	0.01468	0.08947	0.24	1.53	1.34-1.72[a,b,c,e,h]

[a]Reference[Matsushita et al., 2000], [b]Reference[Ã et al., 2005], [c]Reference[Swapna Mary et al., 2016], [d]Reference[Levcenko et al., 2015], [e]Reference[Schleich & Wold, 1977], [f]Reference[Körbel et al., 2015], [g]Reference[Khadka & Kim, 2013], [h]Reference[Swapna Mary, Hema Chandra, Anantha Sunil, & Gupta, 2017], [i]Reference[Nasrin Sarmadian et al., 2016], [j]Reference[León et al., 2010]

The real parts of dielectric function start showing negative value near 8 eV. In this region, the material is showing a metallic nature i.e. a reflective material with the onset of plasmon effect. The corresponding energy and frequency are terms as plasmon energy and plasmon frequency. The values of plasmon energy are ~ 8.7 eV and ~ 8.1 eV for kesterite CZGS/Se and ~ 8.4 eV and ~ 7.7 eV for stannite CZGS/Se materials.
The behavior of imaginary dielectric function is similar to the optical absorption. The threshold value of optical absorptions can be estimated from the variation of imaginary part of dielectric function and is closely related to the bandgap of the material. The absorption threshold arises due to the transition of carrier from the valence band maxima to the conduction band minima. The main peaks are observed at 2.88 eV, 2.65 eV, 2.61 eV, and 2.16 eV in the visible region, for kesterite CZGS, stannite CZGS, kesterite CZGSe and stannite CZGSe, respectively. The small shift in the absorption peaks is due to the relative change in their bandgap values as well the hybridization of the atomic orbitals. The absorption peaks are directly related to the density of states spectra. The observed absorption peaks in the optical spectra arises due to the transition of charge carriers from Cu-d, and S/Se-p states in the valence band to Ge-s and S/Se-p states in the conduction band.

The refractive index and extinction coefficient are computed using the real and imaginary part of the dielectric function using the following expressions:

$$n + ik = \sqrt{Re\,\varepsilon + i\,Im\,\varepsilon}$$

$$\text{Refractive index } (n) = \sqrt{\frac{1}{2}\left[\sqrt{(Re\,\varepsilon)^2 + (Im\,\varepsilon)^2} + Re\,\varepsilon\right]}$$

$$\text{Extinction coefficient } (k) = \sqrt{\frac{1}{2}\left[\sqrt{(Re\,\varepsilon)^2 + (Im\,\varepsilon)^2} - Re\,\varepsilon\right]}$$

The calculated refractive index and extinction coefficient are plotted in **Figure 8.6**. Static refractive index is computed by averaging of all the crystallographic directions using the equation $n_0 = \sqrt{\varepsilon_s(0)}$ and the values summarized in **Table 8.2**. Refractive index is insensitive for initial few electron volts lower energy range and start increasing afterwards because of probable electronic transitions from valence band to conduction band. The qualitative behavior of refractive index is nearly same for kesterite and stannite CZGS/Se phases due to their similar atomic configurations. The static dielectric constant has inverse relationship with bandgap of material which can be explained using Penn model [Penn, 1962] $Re\,\varepsilon(0) \approx 1 + \left(\frac{\hbar\omega_P}{E_g}\right)^2$.

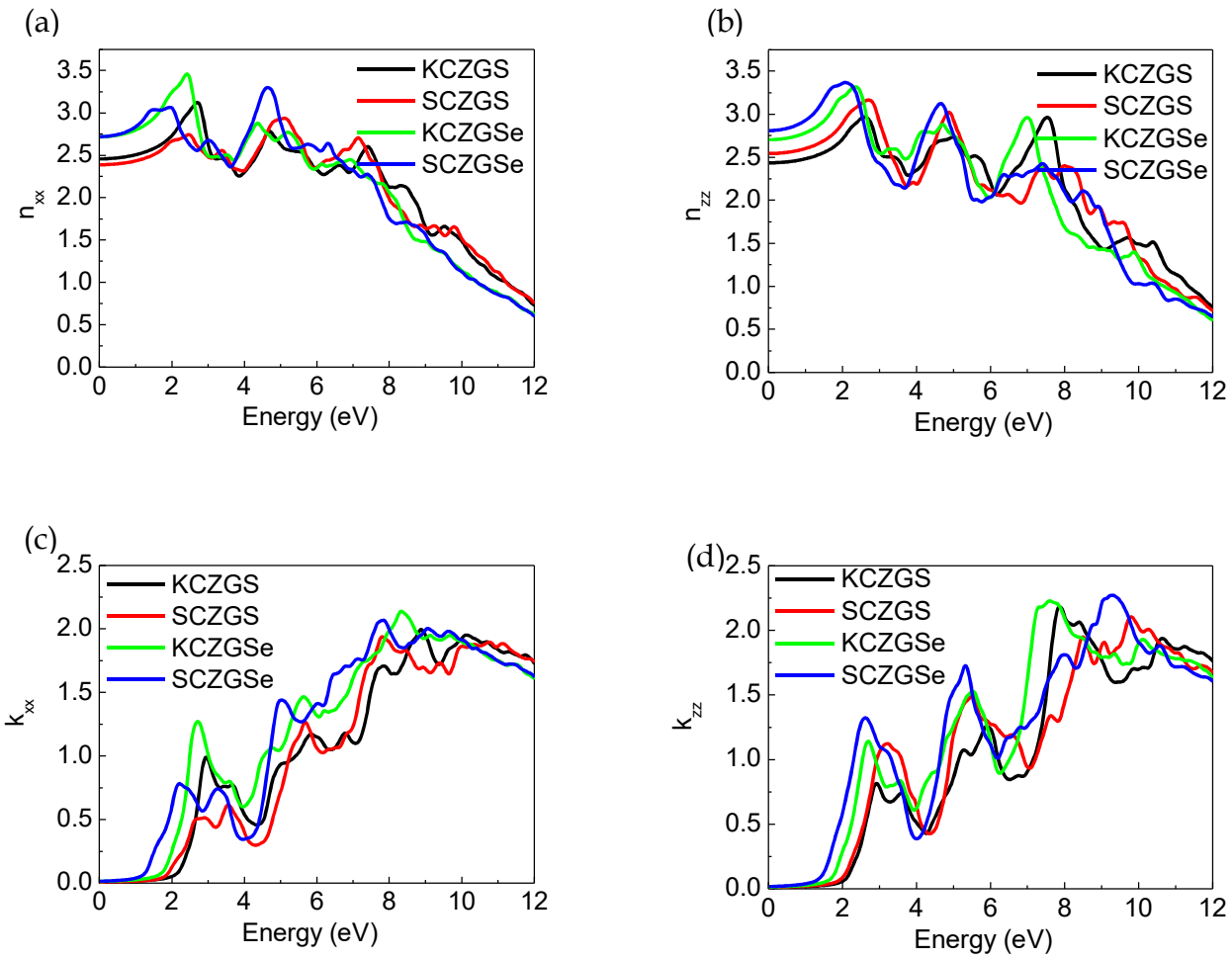

Figure 8.6 Refractive index and extinction coefficient for CZGS/Se in kesterite and stannite phases (a) n_{xx} (b) n_{zz} (c) k_{xx} and (d) k_{zz}

The absorption spectrum and optical conductivity are also important properties of a material for various applications. **Figure 8.7** depicts the computed optical absorption and optical conductivity. The noticed high absorption suggests that these materials may ba potential candidate for photovoltaic applications in their kesterite and stannite phases. The threshold values of these optical absorptions are equal to their respective bandgap values of the material

and peaks observed in spectrum are attributed to the presence of interband transitions of carrier from occupied states (valence band) to unoccupied state (conduction band).

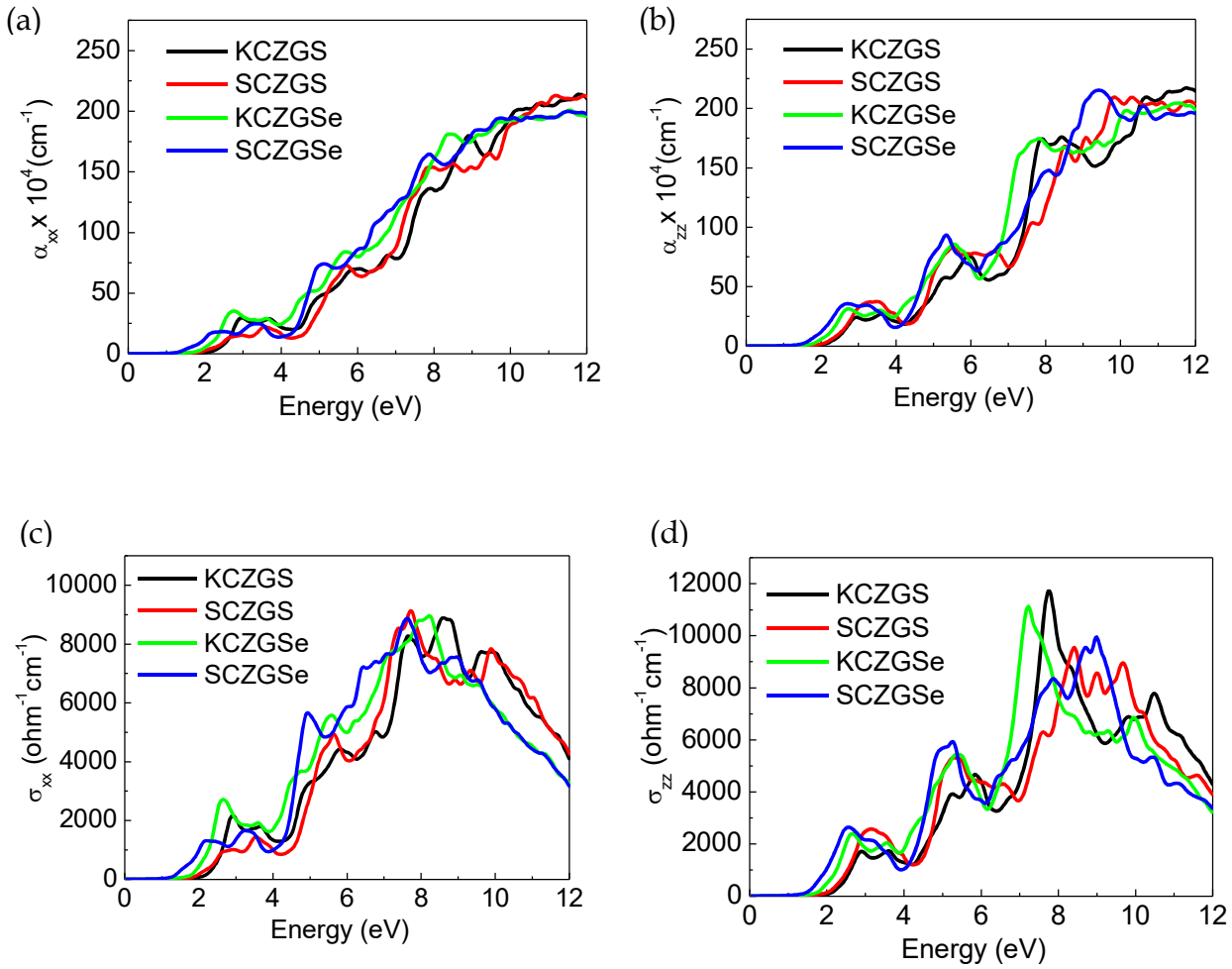

Figure 8.7 Optical absorption and optical conductivity of CZGS/Se in kesterite and stannite phase (a) α_{xx} (b) α_{zz} (c) σ_{xx} and (d) σ_{zz}

Optical absorption spectra are further used to compute the optical bandgap of materials using Tauc plot shown in **Figure 8.8**. The optical bandgap are predicted by extrapolating the linear portion of the $(\alpha h\upsilon)^2 = h\upsilon - E_g$ and the computed values are listed in **Table 8.3.2** for kesterite and stannite CZGS/Se systems. The computed bandgap values are much closer to the experimentally reported values, as listed in **Table 8.2**. The minimum bandgap is observed for stannite CZTSe ~ 1.5 eV and the maximum bandgap are observed ~ 2.1 eV for kesterite CZGS crystallographic phase.

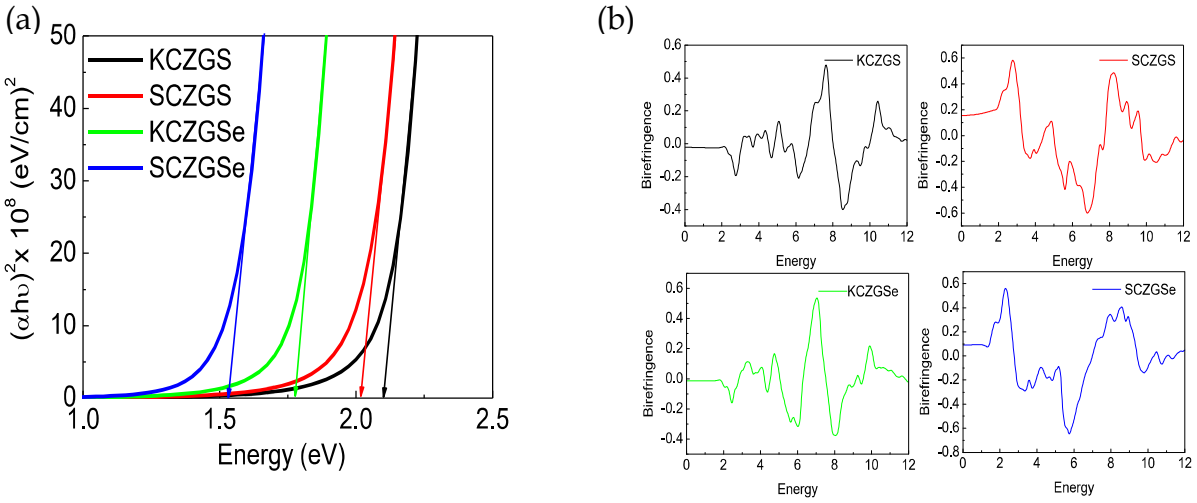

Figure 8.8 (a) Optical band gap of kesterite and stannite phase CZGS/Se after scissor correction of 1 eV in mBJ calculation (b) Birefringence in kesterite and stannite phase CZGS/Se

Optical conductivity of material is directly proportional to the imaginary part of the dielectric function and is expressed as $\sigma = \varepsilon_0 \, (Im\, \varepsilon)\, \omega$; where ε_0 is the absolute permittivity and ω is frequency. The birefringence (Δn) is computed by taking the difference of refractive index along and perpendicular to the c axis. It defines the degree of anisotropy in kesterite and stannite phase of CZGS/Se system shown in **Figure 8.8 (b)**. The positive values of birefringence, observed in case of stannite phase are relatively larger as compared to that of kestarite phase. The observed birefringence value at zero frequency is listed in **Table 8.2**.

Reflectivity are calculated using the expression as $R = \frac{(n-1)^2+k^2}{(n+1)^2+k^2}$; where n is the refractive index and k is the extinction coefficient. The computed reflectivity values along xx and zz directions are shown in **Figure 8.9** for kesterite and stannite CZGS/Se systems. The small values of reflectivity against energy is substantiating that it can be used as a good absorber material for photovoltaic application. The maximum reflectivity values are observed at relatively higher energies, where these materials start showing plasmonic behavior like a metal.

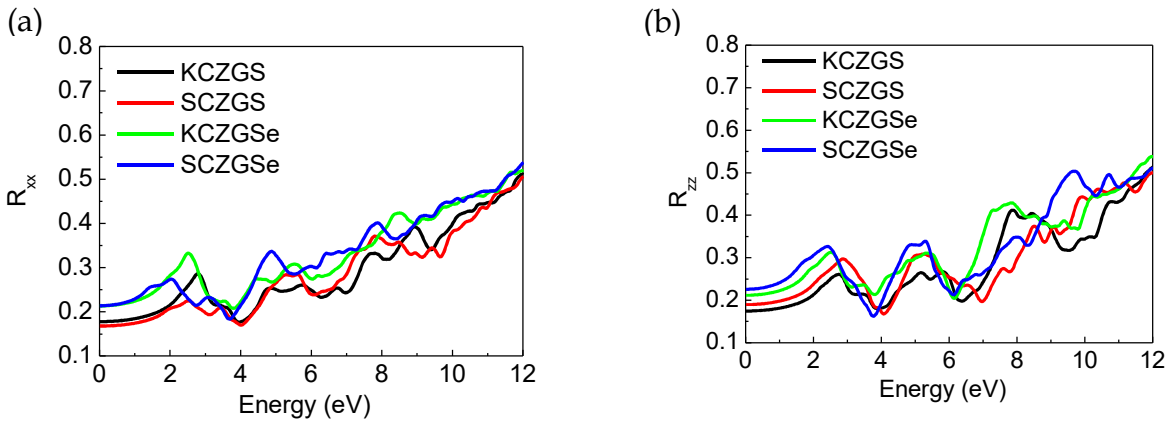

Figure 8.9 Reflectivity components as a function of energy for kesterite and stannite CZGS/Se phases in (a) perpendicular R_{xx} and (b) parallel R_{zz} to tetragonal c-axis

8.4 Conclusion

Electronic and optical properties of CZGS/Se are investigated with mBJ exchange-correlation functional. The computed electronic bandgap confirms the direct bandgap characteristics for both kesterite and stannite CZGS/Se phases. The computed optical properties agree well with the reported experimental and theoretical findings after scissor correction of about 1 eV. The noticed high absorption coefficient makes these materials a suitable choice for thin film photovoltaic single junction and as a top cell absorber material for the tandem cell structures.